Supporting Information for

Use of decoration method on silica nanoparticles to determine element-dependent mitochondria dysfunction

Sojin Kim, Wan–Kyu Oh, Inkyu Lee, and Jyongsik Jang *

WCU program of Chemical Convergence for Energy and Environment (C2E2), School of Chemical and Biological Engineering, College of Engineering, Seoul National University, 599 Gwanak-ro, Gwanak-gu, Seoul 151-742, Korea

[*] E-mail: jsjang@plaza.snu.ac.kr
Tel.: +82-2-880-7069
Fax: +82-2-888-1604

1. Experimental details

1.1 Fabrication of nanodomain decorated SiO_2 nanoparticles (ND-SiO_2 NPs)

SiO_2 NPs were prepared by the Stöber method.[1] First, 2.3 mL of tetraethyl orthosilicate (TEOS; Aldrich, St. Louis, MO) was added to the mixture of ethanol (60.0 mL), ammonium hydroxide solution (3.0 mL), and water (1.0 mL). The sol-gel reaction was carried out for 6 h at 55 °C. In order to capture the precursor ions on their surface, 160 mg of SiO_2 NPs were treated with equivalent weight of N-[3-(trimethoxysilyl)-propyl] ethylenediamine (Aldrich, St. Louis, MO) in 1:1 ethanol-water mixture for 12 h. Fabricating NPs (amine-SiO_2 NPs) were then washed several times. Subsequently, 5 mg of amine-SiO_2 NPs was added to the precursor solutions with vigorous stirring for 12 h at 20 °C. To decorate equivalent weight percentage of the NDs on the SiO_2 NPs, the detailed experimental conditions were slightly different between ND types due to their properties and summarized in Table 1. The metal ions (iron, zinc, copper, and cerium ions) were dissolved in ethanol and coordinated with the diamine species on the surface of the SiO_2 NPs. NaOH was introduced dropwise into precursor solutions, and all reactions were carried out for 12 h at RT. In case of SeO_2, they formed H_2SeO_3 solutions after dissolving in distilled water. The SeO_3^{2-} ions were decorated on the surface of the amine-SiO_2 NP by charge-charge interactions, and reduced by ascorbic acid for 6 h at RT. In case of the MnO_2 NDs, the MnO_4^- ions, located on the surface of the SiO2 NPs by charge-charge interactions, were reduced by formamide for 8 h at 40 °C.

The images and the crystallinity of the NDs were acquired by high resolution transmission electron microscopy (HRTEM; JEOL JEM-3010) and X-ray diffraction (XRD; M18XHF SRA, MAC Science Co.), respectively. Size distribution and zeta potential (ζ) of the ND-SiO_2 NPs

were measured by an ELS-8000 instrument (Otsuka Electronics, Japan). The amount of NDs on SiO_2 NPs was investigated using inductively coupled plasma emission spectrometer (ICP-MS; JP/ICPS-7500, Shimdzu). The oxidation state of CeO_2 was confirmed by X-ray photoelectron spectroscopy (XPS; AXIS- His, KRATOS). Dissolution of metal ions from ND-SiO_2 NPs was measured in DI water and cell culture medium as a function of a time using ICP-MS. ND-SiO_2 NPs were suspended in above mentioned solvents with moderate stirring (20 μg mL^{-1}). Each sample (0.5 mL) was extracted as a function of a time by centrifugation at 10000 rpm for 5 min. The supernatant was transferred to a fresh vial, diluted 10 times with appropriate solvents, and analyzed by above mentioned ICP-MS.

Table S1. Detailed experimental conditions for fabricating ND-SiO_2 NPs

	Precursor and their concentration[a]	Catalyst or reducing agent and their concentration[a]
Ce-SiO_2	$Ce(NO_3)_3 \cdot 6H_2O$, 10 mM	NaOH, 15 mM
Se-SiO_2	SeO_2, 62 mM	Ascorbic acid, 50 mM
Cu-SiO_2	$CuCl_2$, 12 mM	NaOH, 24 mM
Fe-SiO_2	$FeCl_3 \cdot 6H_2O$, 12 mM	NaOH, 36 mM
Mn-SiO_2	$KMnO_4$, 10 mM	$HCONH_2$, 24 mM
Zn-SiO_2	$ZnCl_2$, 15 mM	NaOH, 53 mM

[a]All of them were purchased from Aldrich and used without further purification.

1.2. Three cell lines were used for the nanotoxicological evaluation

Mouse macrophage RAW264.7, rat pheochromocytoma PC12, and calf pulmonary artery endothelial CPAE cell lines were used to investigate the effects of ND-SiO_2 NPs. Macrophages are involved in the first-line immune defense and act as scavengers of foreign agents *via* phagocytosis.[2] PC12 serve as a model system for primary neuronal cells because of their ability

to differentiate in response to nerve growth factors.[3] CPAE are used as blood vessel model system given their origin and ability to respond to vasicular endothelial growth factor.[4] A nanotoxicological evaluation using these three cell lines can provide a comprehensive assessment of the toxic effects of ND-SiO_2 NPs on various organs.

1.3. Cell culture

Cells were obtained from American Type Culture Collection (ATCC, Manassas, USA). RAW264.7 were cultured in Dulbecco's modified eagle medium (DMEM) with 10% fetal bovine serum (FBS), 1% penicillin-streptomycin solution (P/S solution). PC12 were grown in RPMI-1640 medium with 10% horse serum (HS), 5% FBS, and 1% P/S solution. CPAE were maintained in RPMI-1640 with 10% FBS, and 1% P/S solution. Cells were incubated in a 5% CO_2 incubator at 37 °C (100% humidity).

1.4. Internalization of the ND-SiO_2 NPs

Cells were placed in sterile culture dishes (Nunc, Thermo Fisher Scientific, USA) for 24 h, and the ND-SiO_2 NPs (25 μg mL^{-1}) were added for another 24 h. After being washed with 0.1 M PBS, cells were prefixed with Karnovsky's fixative (2% paraformaldehyde and 2% glutaraldehyde), postfixed with 1% OsO_4 for 2 h, and stained with 0.5% uranyl acetate for overnight. Dehydration was conducted through a gradient ethanol and propylene oxide. Then, they were infiltrated in Spurr's resin and hardened at 70 °C for 1 day. The sections were stained with 2% uranyl acetate and Raynolds' lead citrate, and cellular internalization of ND-SiO_2 NPs was observed by TEM (JEM1010, JEOL, Tokyo, Japan).

1.5. Viability test

The viability of the ND-SiO_2 NP-treated cells was measured using Cell-Titer glow luminescent cell viability assay (Promega, Madison, WI, USA). This assay is a homogeneous method of estimating the number of viable cells based on amount of adenosine triphosphate (ATP) in metabolically active cells. For the assay, $1.5x10^4$ cells were seeded in white opaque 96-well plates and treated with different concentrations of the ND-SiO_2 NPs (10, 25, 100, 250, and 500 μg mL^{-1}) for 24 h. After incubation, supernatant was removed and following steps were carried out as supplier's instructions. Cell viability was detected by Victor^3 Multilabel Readers (Perkin Elmer, Boston, MA, USA).

1.6. ROS production and loss of mitochondrial membrane potential (MMP)

Cells were plated in 6 well plates at a density of $1x10^5$ cells mL^{-1} and treated with ND-SiO_2 NPs (10, 25, 100, 250, and 500 μg mL^{-1}) each for 24 h. The cells were washed, trypsinized, and collected in tubes. After being resuspended in 0.1 M HBSS (Hank's Buffered Salt Solution), the cells were incubated with MitoSOX (to measure the mitochondrial superoxide) or H_2DCFDA (to measure total cellular H_2O_2) (Invitrogen, Grand Island, NY, USA) at 5 μM concentration for 15 and 30 min at 37 °C, respectively. In case of MMP, cells were stained with 2.5 μg mL^{-1} JC-1 for 30 min at 37 °C. They were analyzed by FACS Aria I (BD Bioscience, USA).

1.7. Immunocytochemistry

As described above, $1x10^5$ cells were treated with ND-SiO_2 NPs (25 μg mL^{-1}) for 24 h. Being washed with 0.1 M PBS, the cells were fixed with 4% paraformaldehyde for 20 min,

permeabilized with 0.1% Triton X-100 for 15 min, and blocked with blocking solution (0.1 M PBS, 10% FBS, and 0.03% 1 M NaN_3) for 30 min. Divalent metal transporter 1 antibodies (DMT1; Santa Cruz, USA) were diluted with blocking buffer and incubated with cells for 1 h. Then, the cells were stained with FITC conjugated secondary antibodies for 1 h and analyzed with flow cytometry (FACS Aria I, BD Bioscience, USA).

1.8. Apoptosis and necrosis

As described earlier, cells were seeded and treated with ND-SiO_2 NPs (10 μg mL^{-1}) for 24 h. An annexin (aV)/propidium iodide (PI) double staining (Vybrant apoptosis assay kit, Invitrogen, Grand Island, NY, USA) can visualize the apoptotic/necrotic cells, and were conducted as manufacturer's instructions. Live cell images were obtained by Delta Vision RT imaging system (Applied Precision, Issaquah, WA) under CO_2 control (5%) at 37 °C. To obtain apoptosis and necrosis cell images, Cascade II electronmultiplying charge-coupled device (EMCCD) camera was used. For quantification of apoptotic cells, 25 μg mL^{-1} ND-SiO_2 NPs treated cells were stained with ND-SiO_2 NPs, and analyzed using flow cytometry (FACS Aria I, BD Bioscience, USA) at an emission wavelength of 530 nm for aV and 585 nm for PI.

2. Size distribution histograms by ELS

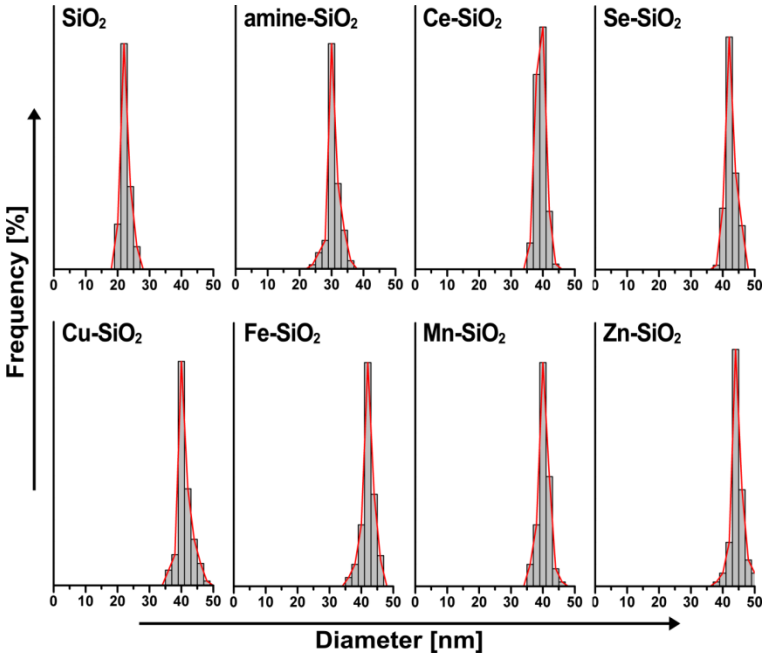

Fig. S1. Size distribution histograms of SiO_2, amine functionalized SiO_2, and ND-SiO_2 NPs determined by ELS.

Fig. S1 illustrates electrophoretic light scattering spectrophotometer (ELS) histograms of SiO_2, amine functionalized SiO_2, and ND-SiO_2 NPs in DI water. Diameter of the SiO_2 NPs, determined by ELS, increased from *ca.* 24 nm to *ca.* 30 nm after silane treatment. The ND-SiO_2 NPs averaged 42 nm in diameter due to NDs on the surface of the SiO_2 NPs. HRTEM images revealed the presence of NDs on the surface of SiO_2 NPs, and each nanodomain was between 4-8 nm in size. The ELS histograms exhibited relatively narrow size distribution of the NPs due to their uniform silica cores, which could be applicable to research for cellular toxicity of the NPs.

3. Crystallinity and chemical composition of the ND-SiO_2 NPs

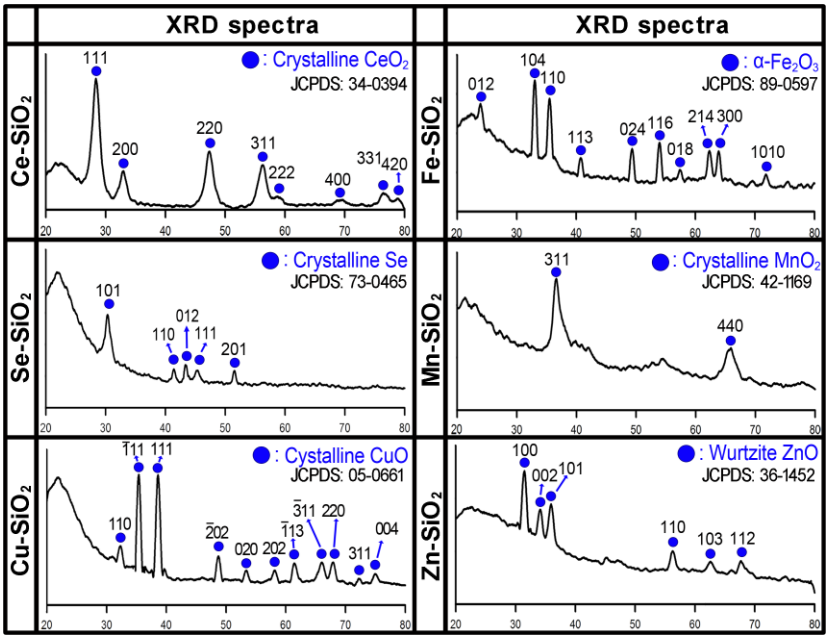

Fig. S2. X-ray diffraction (XRD) spectra of ND-SiO_2 NPs

The chemical composition and crystallinity were analyzed by XRD. A broad peak between 20° and 30° showed the amorphous phase of SiO_2 NPs, and other sharp peaks displayed the crystalline phase of the NDs. A crystalline phase was detected without noticeable contaminants, and the chemical compositions of the NDs were determined by these sharp peaks.

4. Characterizations of ND-SiO_2 NPs

Table S2. Characterizations of ND-SiO_2 NPs

	Chemical composition[a]	Crystallinity [unit cell] [a]	ζ (mV) [b]	ND ratio (wt%)[c]	Dissolution (%)[d]	
					DI water	Medium[e]
SiO_2	N/A	Amorphous	-31.50 ± 3.16	N/A	N/A	N/A
amine-SiO_2	N/A	Amorphous	38.05 ± 4.13	N/A	N/A	N/A
Ce-SiO_2	CeO_2	Crystalline [Cubic]	-16.23 ± 1.13	12.69	7.13	1.22
Se-SiO_2	Se	Crystalline [Trigonal]	-45.54 ± 4.25	13.28	8.90	2.44
Cu-SiO_2	CuO	Crystalline [Monoclinic]	23.02 ± 3.92	12.82	12.60	1.79
Fe-SiO_2	Fe_2O_3	Alpha type [Rhombohedral]	-14.37 ± 3.49	12.05	7.30	3.76
Mn-SiO_2	MnO_2	Crystalline	-11.04 ± 2.23	13.36	6.92	0.84
Zn-SiO_2	ZnO	Wurtzite [Hexagonal]	13.71 ± 1.21	12.06	19.74	6.38

[a]The crystallinity of ND was determined by XRD spectrum. [b]ζ of the ND-SiO_2 NPs in aqueous solution was measured by ELS-8000. [c]The weight ratio of ND in ND-SiO_2 NPs were analyzed by ICP-MS. [d]Dissolution of the NDs was evaluated using ICP-MS at 37 °C in supernatant of the water and culture mediums for 24 h. [e]DMEM with 10% fetal bovine serum, and 1% penicillin-streptomycin solution was used as culture medium.

The physicochemical properties of the NPs were characterized by XRD, ELS, and ICP-MS (Table S2). The zeta potential (ζ) also provided evidence for the presence of NDs on the NP surface. Bare SiO_2 NPs were negatively charged, whereas the amine-SiO_2 NPs had a positive charge. After formation of the NDs, the ζ of the NPs decreased due to the negative surface charge of the NDs. The amount of ND on the SiO_2 NPs was calculated as an average 12-13 wt% by ICP-MS. This method enabled us to evaluate and compare the precise nanotoxicity of various element NDs on the surface of silica NPs. To the best of our knowledge, this is the first attempt to compare nanomaterials as nanodomain with controlled physical properties on the SiO_2 NPs for

precise nanotoxicity. We further investigated the dissolution of NDs in distilled water and cell culture medium to estimate the effect of dissolved ions on cellular toxicity. About 7-9% of the NDs were leached as ions in distilled water, whereas 12.6% and 19.7% of the Cu-SiO_2 and Zn-SiO_2 NP dissolved, respectively. The dissolution of the NDs was decreased in culture medium due to the colloidal stability effects of the solvents.[5] Dissolved Cu^{2+} ions decreased from 12.6% to 1.79%, which was consistent with the other ND-SiO_2 NPs except Zn-SiO_2 NPs. In case of Zn-SiO_2 NP, the released ions was still over 6% even in culture medium. Several papers reported that unlike other nanomaterials, nanosized ZnO undergoes rapid dissolution in cell culture medium, which was good agreement with our results.[6] To compare the dissolution of ND inside of cell organelles, leached metal ions were quantified in a lysosomal buffer solution which is similar condition with lysosomes. In lysosomal buffered solution, *ca.* 40% of Zn^{2+} ions was leached from Zn-SiO_2 NPs, which is 6 times higher than in cell culture medium (data not shown). In case of the Zn-SiO_2 NPs, it can be concluded that the effects of ND on SiO_2 NPs are dominant on the Zn-SiO_2 NP toxicity and the metal ion dissolution are considered as minor factor.

5. Uptake of ND-SiO_2 NPs

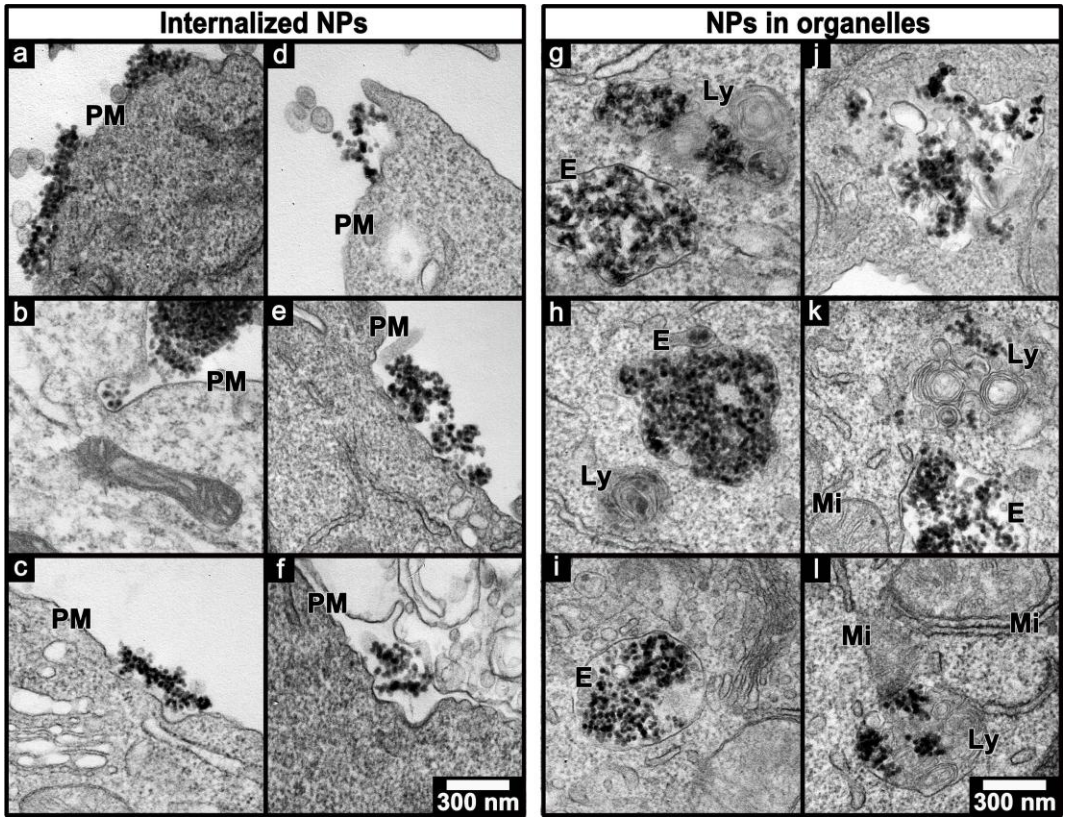

Fig. S3. TEM images of RAW264.7 cells treated with 25 μg mL^{-1} of ND-SiO_2 NPs for 24 h. (a, g) Ce-SiO_2; (b, h) Se-SiO_2; (c, i) Cu-SiO_2; (d, j) Fe-SiO_2; (e, k) Mn-SiO_2; (f, l) Zn-SiO_2. Abbreviations: PM, the plasma membrane; E, endosome; Mi, the mitochondria; Ly, the lysosome.

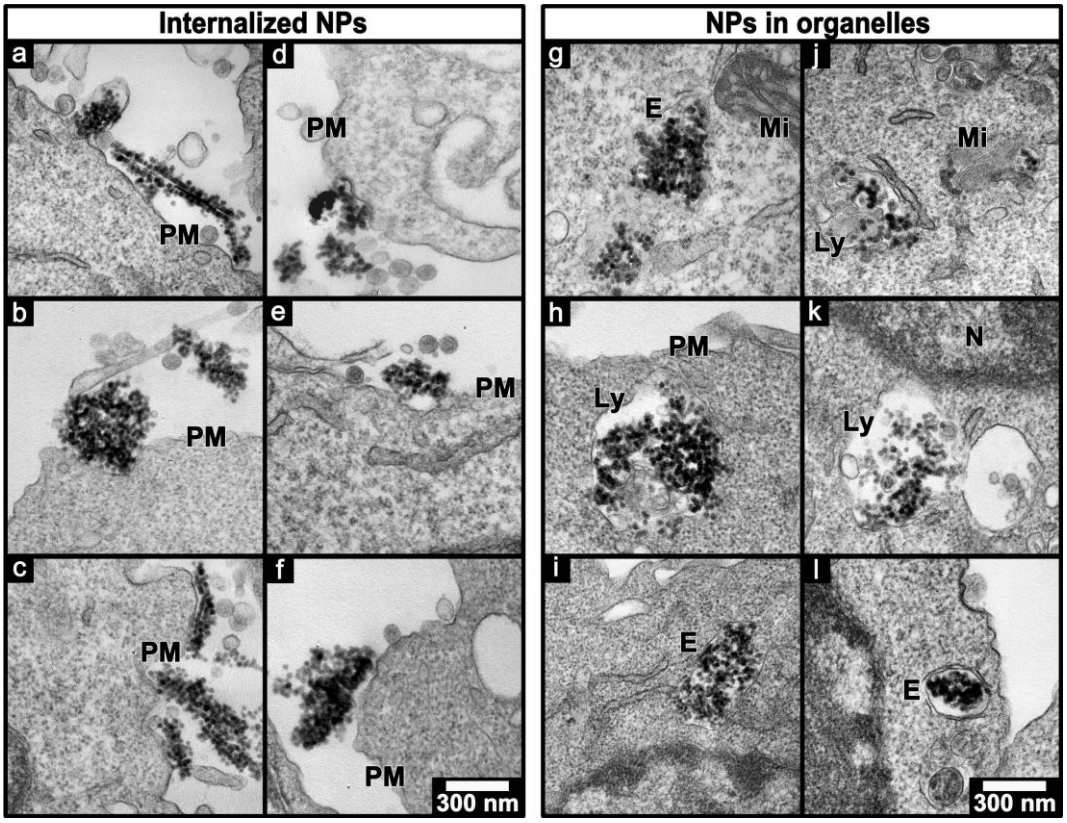

Fig. S4. TEM images of PC12 cells treated with 25 μg mL^{-1} of ND-SiO_2 NPs for 24 h. (a, g) Ce-SiO_2; (b, h) Se-SiO_2; (c, i) Cu-SiO_2; (d, j) Fe-SiO_2; (e, k) Mn-SiO_2; (f, l) Zn-SiO_2. Abbreviations: PM, the plasma membrane; N, nucleus; E, endosome; Mi, the mitochondria; Ly, the lysosome.

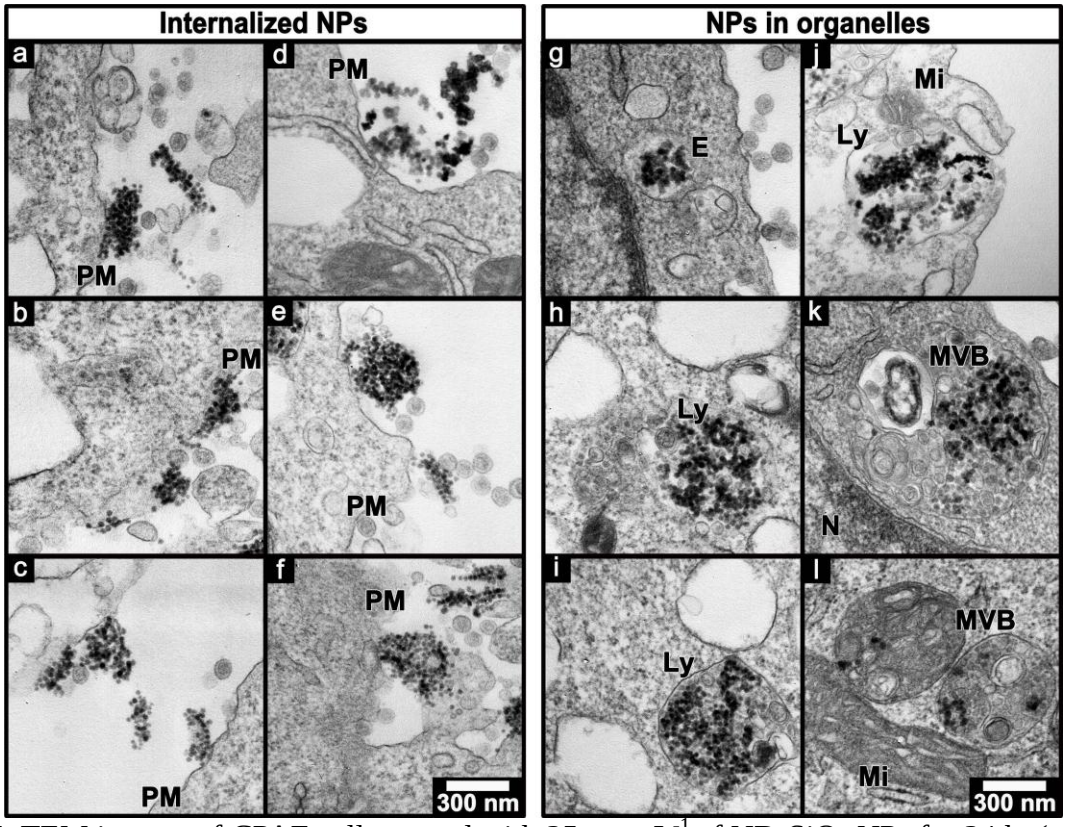

Fig. S5. TEM images of CPAE cells treated with 25 μg mL^{-1} of ND-SiO_2 NPs for 24 h. (a, g) Ce-SiO_2; (b, h) Se-SiO_2; (c, i) Cu-SiO_2; (d, j) Fe-SiO_2; (e, k) Mn-SiO_2; (f, l) Zn-SiO_2. Abbreviations: PM, the plasma membrane; N, nucleus; E, endosome; Mi, the mitochondria; MVB, multivesicular bodies; Ly, the lysosome.

The cellular uptake of ND-SiO_2 NPs was observed by TEM, and representative images are shown (Fig. S3-S5). Clustered NPs were attached to the plasma membrane, and internalized NPs were distributed throughout the cytoplasm. No significant difference in cellular uptake was observed among the cell-type and ND-type. Invaginations of the cell plasma membrane were observed during ND-SiO_2 NPs internalization. Invagination and protrusion of the plasma membranes denote endocytosis and macropinocytosis, respectively. Thus, both mechanisms were used simultaneously for cellular uptake of ND-SiO_2 NPs. Internalized nanomaterials are delivered from the plasma membrane to several organelles *via* multiple pathways, but the exact mechanism has not been determined.[7, 8]

ND-SiO_2 NPs were found in endosomes, multivesicular bodies, and lysosomes, indicating that most of the internalized ND-SiO_2 NPs were transported *via* the endosome network which consists of endosomes, multivesicular bodies, and lysosomes. The ND-SiO_2 NPs did not penetrate into nor interact with the Golgi apparatus or the nucleus. ~~After internalization, most of the internalized ND-SiO_2 NPs were transported *via* the endosome network which consists of endosomes, multivesicular bodies, and lysosomes.~~ This result was consistent with the cellular uptake model suggested by previous reports.[9] Interestingly, some of lysosomes containing the ND-SiO_2 NPs were damaged, swelled (the blue arrow in Fig. 2c), and even ruptured (the black arrow in Fig. 2c). Several studies hav e reported that NPs in lysosome undergo intracellular excretion by lysosomal rupture.[10] T he pH inside the lysosomes is 4.7, which is capable of ionizing NDs on the surface of Si O_2 NPs.[11] Some of the metal ions passed through the lysosomal membrane and were rele ased into the cytosol, but the remaining ions have the potential to cause lysosomal dama ges, swelling, even rupture. When NPs were released from the lysosome to the cytoplas m through the ruptured membrane, the released ND-SiO_2 NPs were freely dispersed and moved to the mitochondria.[8] In case of the mitochondria which are distant from the NPs, cristae and intact outer membrane structure was clearly observed (red arrows in Fig, 2b). However, when the Fe-SiO_2 NPs, released from the lysosomes, existed near the mitochondria (yellow arrows in Fig. 2d), the half of mitochondria outer membrane was disappeared (Fig. 2d). Compared with Fig. 2b and 2d, the mitochondria near the NPs appeared to be damaged, su ggesting that the released NPs might have affected mitochondria function. Therefore, we focused on the mitochondrial dysfunction affected by ND-SiO_2 NPs.

6. Classification of the ND-SiO_2 NPs

Table S3. Classification of the ND-SiO_2 NPs according to their toxicity

	Species	Origin	Group I[a]	Group II[b]	Group III[c]
RAW264.7	Mouse	Macrophage	Ce-SiO_2	Se-SiO_2 Cu-SiO_2 Fe-SiO_2 Mn-SiO_2	Zn-SiO_2
PC12	Rat	pheochromocytoma	Ce-SiO_2	Se-SiO_2 Cu-SiO_2 Fe-SiO_2	Mn-SiO_2 Zn-SiO_2
CPAE	Calf	pulmonary artery endothelial	Ce-SiO_2	Se-SiO_2 Cu-SiO_2	Fe-SiO_2 Mn-SiO_2 Zn-SiO_2

[a]The Group I is less cytotoxic than that of bare SiO_2 NPs. [b]The Group II shows similar toxicity to bare SiO_2 NPs. [c]The Group III is more toxic than that of bare SiO_2 NPs.

7. Mitochondria dysfunction by the Group III treatments

Among the metal ions in Group III, Zn^{2+} can affect cellular respiration by interfering with cytochrome *bc1* (complex III) and cytochrome *c* oxidase (complex IV) complexes of the mitochondrial respiratory electron transport chain and can inhibit α-ketoglutarate-simulated respiration.[12] The produced $O2^{\cdot -}$ by causing mitochondrial dysfunction can generate $ONOO^-$, which in turn amplifies the oxidation of Zn-S bridges in metallothionein, a major Zn^{2+} reservoir, and thus generations additional Zn^{2+}.[13] Moreover, the Zn^{2+}, similar to Ca^{2+}, has a direct effect on mitochondria by inducing the opening of the mitochondrial permeability transition pore and release of cytochrome *c* from mitochondria, thereby disrupting mitochondrial function.[13]

Mn^{2+} enter mitochondria *via* the Ca^{2+} uniporter and interfere with cellular respiration by inhibiting both F1-ATPase and the citric acid cycle enzyme aconitase.[14] Additionally, Mn^{2+} directly inhibits Na^+-dependent and -independent Ca^{2+} transporters in the mitochondrial membrane, causing activation of the mitochondrial permeability transition pore and cytochrome *c* release.[15] The Fe^{2+}/Fe^{3+} redox potential is compatible with the constraints of the cellular environment; however, this property converts iron into a potential biohazard.[16, 17] Owing to the redox and catalytic properties of iron, its toxicity is based primarily on ROS generation.

Fe^{2+} can cross the mitochondria membrane and react with hydrogen peroxide and oxygen, generating highly reactive hydroxyl and superoxide radicals *via* Fenton and Haber–Weiss chemistry.[17] Redox-active iron catalyzes the generation of not only hydroxyl radicals but organic reactive species such as peroxyl, or alkoxyl radicals. Similar to Mn^{2+}, Fe^{2+} ions also inhibit aconitase.[16]

8. Cellular protection against exogenous source of ROS by Ce-SiO_2 NPs

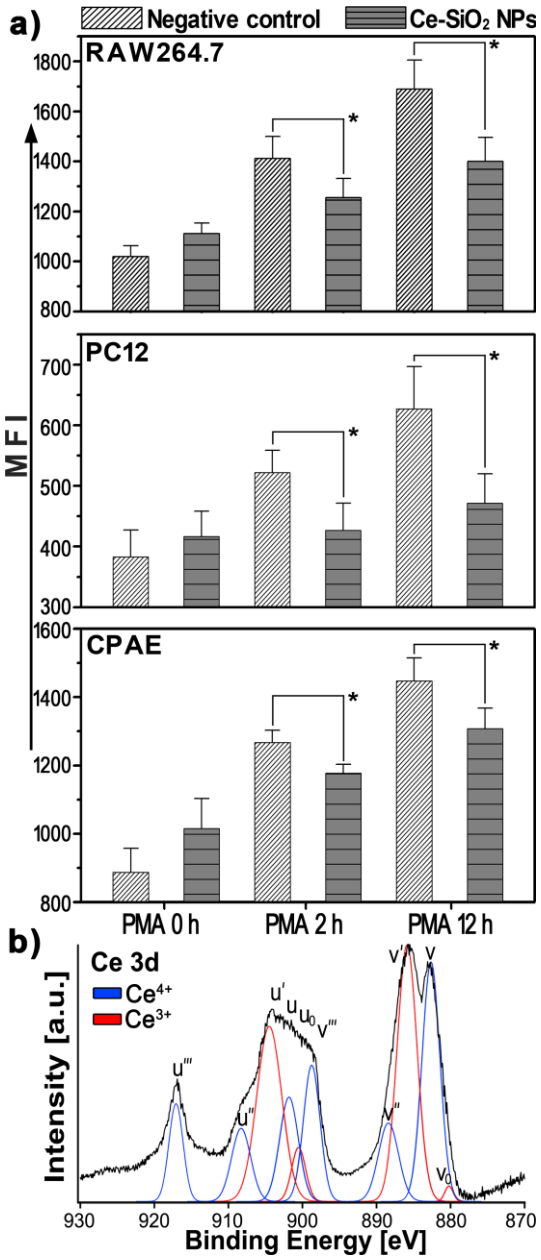

Fig. S6. a) Protective effect of the Ce-SiO_2 NPs on PMA induced ROS in the cells. The cells were pretreated with 25 μg mL^{-1} Ce-SiO_2 NPs for 24 h, followed by addition of 1 μg mL^{-1} of PMA for 0, 2, and 12 h. The PMA plays a role as ROS inducer in cells. Among graphs, free of NPs in the cells was used as a negative control. Values exhibit mean ± SD and independent experiments were performed three times (n=3). The asterisk (*) denoted a statistically significant difference from the bare-SiO_2 treated cells to the ND-SiO_2 NP treated cells ($P < 0.05$). b) XPS spectrum of Ce-SiO_2 NP. Two sets of spin-orbital multiplets, corresponding to the $3d_{3/2}$ and $3d_{5/2}$, were labeled as u and v, respectively.

Cells treated with Ce-SiO_2 NPs produced more ATP and less ROS than those treated with SiO_2 NPs (Fig. 2 and Fig. 3a-c). We hypothesized that CeO_2 on the SiO_2 NPs could also protect cells against oxidative damages from an exogenous ROS source. To verify this hypothesis, cells were pretreated with 25 μg mL^{-1} of Ce-SiO_2 NPs for 24 h, followed by treatment with phorbol 12-myristate 13-acetate (PMA; 1 μg mL^{-1}) for 0, 2, and 12 h. A previous work has shown that PMA are inducing intracellular ROS generation.[18] As shown in Fig. S6a, ROS production was greater in the Ce-SiO_2 NP-treated cells than in the control at 0 h of PMA treatment. However, treatment with PMA decreased ROS generation in the Ce-SiO_2 NP-incubated cells. When the Ce-SiO_2 NPs and PMA were added simultaneously to the cells in a control experiment, no particular protective effect was observed (data not shown). Therefore, the Ce-SiO_2 NPs had to be internalization prior to the addition of PMA to achieve a protective effect. These results suggest that CeO_2 NDs SiO_2 NPs can reduce not only SiO_2 own toxicity but also ROS production in the presence of an exogenous ROS sources.

Several studies have demonstrated that CeO_2 can scavenge free radicals, resulting in an antioxidant effect in cells.[19] This property is attributable primarily to the reversible Ce^{3+}/Ce^{4+} redox couple, not the oxygen vacancies.[19] Possible reactions involving radical quenching and redox coupling reaction between Ce^{3+} and Ce^{4+} are shown below. These equations explained how the Ce^{3+}/Ce^{4+} mixed oxidation state are required for radical scavenging.

$$Ce^{3+} + O_2^{\cdot -} + 2H^+ (aq) \rightarrow Ce^{4+} + 2H_2O_2 \qquad (1)$$

$$2\ Ce^{4+} + 2H_2O_2 \rightarrow 2\ Ce^{3+} + 2H^+ + O_2^{\cdot} \qquad (2)$$

In order to explain the antioxidant effects of CeO_2 NDs on SiO_2 NPs, the oxidation state of CeO_2 was confirmed using XPS analysis (Fig. S6b). The Ce 3d spectra were based on prior research; two sets of spin-orbital multiplets, corresponding to $3d_{3/2}$ and $3d_{5/2}$, were labeled as u and v, respectively.[20] The Ce 3d spectra of the Ce-SiO_2 NPs were deconvoluted as myriad peaks, indicating that the CeO_2 NDs consisted of a mixture of Ce^{3+} and Ce^{4+} oxidation states. CeO_2 undergoes easy, fast, and reversible reduction and can readily take up and release oxygen, alternating between CeO_2 and CeO_{2-X}.[21] Thus, the protective effects of CeO_2 NDs on SiO_2 NPs originate from its mixed Ce^{3+}/Ce^{4+} oxidation states, in accordance with reported data. As contrasted with Ce-SiO_2 NPs, other ND-SiO_2 NP had no scavenging ability for free radicals.

9. Cell death mechanism

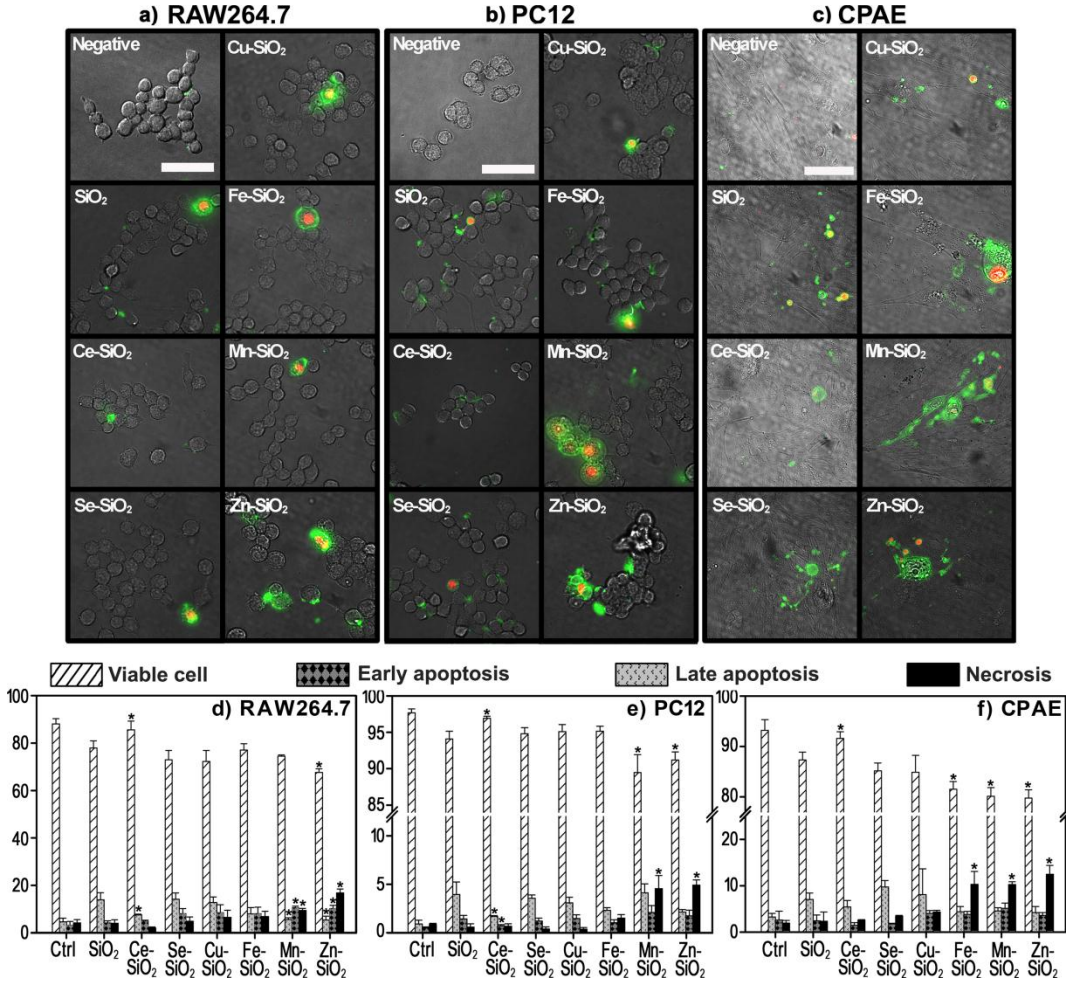

Fig. S7. Determination of apoptosis and necrosis by a-c) fluorescence images and d-f) flow cytometric analysis. The cells were treated with ND-SiO_2 NPs (25 μg mL^{-1}) for 24 h, and stained with annexin V (green)/propidium iodide (red). a-c) Unstained and dual-stained cells were presented viable and late apoptotic cells. The green/red fluorescent labels represent as early apoptotic/necrotic cells (scale bars: 20 μm). d-f) Apoptosis and necrosis ratio was measured by flow cytometry. Free of the NPs in the cells was used as a control (Ctrl). Values exhibit mean ± SD and each experiment was performed in triplicate. The asterisk (*) denoted a statistically significant difference from the SiO_2 treated cells exposed to the ND-SiO_2 NP treated cells ($P < 0.05$).

10. References

1. C. Kim, S. Kim, W.-K. Oh, M. Choi and J. Jang, *Chem. Eur. J.*, 2012, **18**, 4902.
2. S. L. Montes-Fonseca, E. Orrantia-Borunda, A. Aguilar-Elguezabal, C. González Horta, P. Talamás-Rohana and B. Sánchez-Ramírez, *Nanomed. Nanotechnol. Biol. Med.*, 2012, **8**, 853.
3. J. Wu, C. Wang, J. Sun and Y. Xue, *ACS Nano*, 2011, **5**, 4476.
4. S. Y. Hwang, K. W. Kwon, K.-J. Jang, M. C. Park, J. S. Lee and K. Y. Suh, *Anal. Chem.*, 2010, **82**, 3016.
5. T. Xia, M. Kovochich, M. Liong, L. Mädler, B. Gilbert, H. Shi, J. I. Yeh, J. I. Zink and A. E. Nel, *ACS Nano*, 2008, **2**, 2121.
6. H. Zhang, Z. Ji, T. Xia, H. Meng, C. Low-Kam, R. Liu, S. Pokhrel, S. Lin, X. Wang, Y.-P. Liao, M. Wang, L. Li, R. Rallo, R. Damoiseaux, D. Telesca, L. Mädler, Y. Cohen, J. I. Zink and A. E. Nel, *ACS Nano*, 2012, **6**, 4349; K. H. Müller, J. Kulkarni, M. Motskin, A. Goode, P. Winship, J. N. Skepper, M. P. Ryan and A. E. Porter, *ACS Nano*, 2010, **4**, 6767.
7. A. Nagy, A. Steinbrück, J. Gao, N. Doggett, J. A. Hollingsworth and R. Lyer, *ACS Nano*, 2012, **6**, 4748; T. Hamada, M. Morita, M. Miyakawa, R. Sugimoto, A. Hatanaka, M. d. C. Vestergaard and M. Takagi, *J. Am. Chem. Soc.*, 2012, **134**, 13990.
8. Ž. Krpetić, P. Nativo, I. A. Prior and M. Brust, *Small*, 2011, **7**, 1982.
9. S. Kim, W.-K. Oh, Y. S. Jeong, J.-Y. Hong, B.-R. Cho, J.-S. Hahn and J. Jang, *Biomaterials*, 2011, **32**, 2342.
10. E.-J. Yang, S. Kim, J. S. Kim and I.-H. Choi, *Biomaterials*, 2012, **33**, 6858; M. Mahmoudi, S. Laurent, M. A. Shokrgozar and M. Hosseinkhani, *ACS Nano*, 2011, **5**, 7263.
11. J. R. Casey, S. Grinstein and J. Orlowski, *Nat. Rev. Mol. Cell Biol.*, 2010, **11**, 50.

12. S. L. Sensi, H. Z. Yin, S. G. Carriedo, S. S. Rao and J. H. Weiss, *Proc. Natl. Acad. Sci. USA*, 1999, **96**, 2414.

13. E. Bossy-Wetzel, M. V. Talantova, W. D. Lee, M. N. Schölzke, A. Harrop, E. Mathews, T. Götz, J. Han, M. H. Ellisman, G. A. Perkins and S. A. Lipton, *Neuron*, 2004, **41**, 351.

14. K. M. Erikson, K. Thompson, J. Aschner and M. Aschner, *Pharmacol. Ther.*, 2007, **113**, 369.

15. J. A. Roth and M. D. Garrick, *Biochem. Pharmacol.*, 2003, **66**, 1.

16. G. Papanikolaou and K. Pantopoulos, *Toxicol. Appl. Pharmacol.*, 2005, **202**, 199.

17. N. Singh, G. J. S. Jenkins, R. Asadi and S. H. Doak, *Nano Reviews*, 2010, **1**, 5358.

18. J. R. Henderson, D. A. Fulton, C. J. McNeil and P. Manning, *Biosens. Bioelectron.*, 2009, **24**, 3608.

19. I. Celardo, M. De Nicola, C. Mandoli, J. Z. Pedersen, E. Traversa and L. Ghibelli, *ACS Nano*, 2011, **5**, 4537.

20. B. Reddy and A. Khan, *Catal. Surv. Asia*, 2005, **9**, 155.

21. M. S. Wason, J. Colon, S. Das, S. Seal, J. Turkson, J. Zhao and C. H. Baker, *Nanomed. Nanotechnol. Biol. Med.*, 2013, **9**, 558.